Draft version April 24, 2013
Preprint typeset using LaTeX style emulateapj v. 12/01/06

REDSHIFT 6.4 HOST GALAXIES OF 10^8 SOLAR MASS BLACK HOLES: LOW STAR FORMATION RATE AND DYNAMICAL MASS

Chris J. Willott
Herzberg Institute of Astrophysics, National Research Council, 5071 West Saanich Rd, Victoria, BC V9E 2E7, Canada

Alain Omont and Jacqueline Bergeron
UPMC Univ Paris 06 and CNRS, UMR7095, Institut d'Astrophysique de Paris, F-75014, Paris, France
Draft version April 24, 2013

ABSTRACT

We present ALMA observations of rest-frame far-infrared continuum and [C II] line emission in two $z = 6.4$ quasars with black hole masses of $\approx 10^8 M_\odot$. CFHQS J0210-0456 is detected in the continuum with a 1.2 mm flux of $120 \pm 35\,\mu$Jy, whereas CFHQS J2329-0301 is undetected at a similar noise level. J2329-0301 has a star formation rate limit of $< 40\,\mathrm{M_\odot\,yr^{-1}}$, considerably below the typical value at all redshifts for this bolometric luminosity. By comparison with hydro simulations, we speculate that this quasar is observed at a relatively rare phase where quasar feedback has effectively shut down star formation in the host galaxy. [C II] emission is also detected only in J0210-0456. The ratio of [C II] to far-infrared luminosity is similar to that of low redshift galaxies of comparable luminosity, suggesting the previous finding of an offset in the relationships between this ratio and far-infrared luminosity at low- and high-redshift may be partially due to a selection effect due to the limited sensitivity of previous continuum data. The [C II] line of J0210-0456 is relatively narrow (FWHM $= 189 \pm 18\,\mathrm{km\,s^{-1}}$), indicating a dynamical mass substantially lower than expected from the local black hole – velocity dispersion correlation. The [C II] line is marginally resolved at $0\farcs7$ resolution with the blue and red wings spatially offset by $0\farcs5$ (3 kpc) and a smooth velocity gradient of $100\,\mathrm{km\,s^{-1}}$ across a scale of 6 kpc, possibly due to rotation of a galaxy-wide disk. These observations are consistent with the idea that stellar mass growth lags black hole accretion for quasars at this epoch with respect to more recent times.

Subject headings: cosmology: observations — galaxies: evolution — galaxies: high-redshift — quasars: general

1. INTRODUCTION

The peak of global star formation occurred about 10 billion years ago at a redshift of $z \approx 2$ (Reddy & Steidel 2009). The rise in star formation at earlier times is studied by tracing the space density and properties of higher redshift galaxies. Such galaxies can be selected in the rest-frame ultraviolet as Lyman break dropouts (Bouwens et al. 2006), in the rest-frame infrared as line or continuum sources (Carilli & Walter 2013), via black hole accretion activity as active galactic nuclei (AGN) or quasars (Fan et al. 2006), or via stellar explosions such as gamma ray bursts (Tanvir et al. 2012). These methods are complementary in that they are sensitive to galaxies with a range of mass, star formation rate, dust formation rate and black hole accretion rate, to allow a broad view of early galaxy evolution.

Thanks to the high fraction of stellar radiation reradiated in the infrared by interstellar dust and gas and the negative k-correction (Blain & Longair 1993), high redshift galaxies can be well studied by millimeter observations. Continuum observations are sensitive to the star formation rate as radiation from young, hot stars is reradiated by dust. Molecular lines such as CO probe the molecular gas in dense star-forming regions. Atomic lines such as the fine-structure line of singly-ionized carbon, [C II], probe the interstellar medium and the outer parts of star-forming regions. It has been recognized that the [C II] line will likely become the most useful line for studying very high redshift galaxies with the Atacama Large Millimeter Array (ALMA; Walter & Carilli 2008). Indeed early ALMA observations already show detections of [C II] in normal star-forming galaxies at $z > 4$ (Wagg et al. 2012; Carilli et al. 2013). [C II] has also been detected in a few $z > 6$ quasar host galaxies (Maiolino et al. 2005; Walter et al. 2009; Venemans et al. 2012; Wang et al. 2013).

One of most puzzling aspects of galaxy evolution is the tight correlation between black hole mass and galaxy properties such as bulge stellar mass and velocity dispersion (Magorrian et al. 1998; Ferrarese & Merritt 2000). This correlation suggests a physical connection between black hole accretion on sub-parsec (pc) scales and galaxy-wide star formation and gas accretion on kiloparsec (kpc) scales. The most likely explanation is quasar feedback, but the details of how this operates as a function of cosmic time are still to be determined (Cattaneo et al. 2009). Observationally, this topic can be studied by measuring the global growth rates of black holes and galaxies and the ratio of black hole to stellar mass in high redshift galaxies. The black hole masses of quasars can be measured from the dynamics of gas in the broad line region which is only ~ 1 pc from the black hole (Wandel 1999).

As well as studying the physical properties of star-forming gas in high-redshift galaxies, millimeter interferometry can be used to probe the gas dynamics. A particularly useful application is that of quasar host

Electronic address: chris.willott@nrc.ca

galaxy dynamical masses to measure the ratio of black hole to galaxy mass in the early universe (Walter et al. 2004). Observations in the rest-frame UV or optical are hampered by the overwhelming brightness of the quasar point-source (e.g. Mechtley et al. 2012). Wang et al. (2010) showed that CO line widths of the most optically luminous $z \approx 6$ quasars indicate ratios of black hole to galaxy mass a factor of 10 on average greater than found in the local universe. This could signal that black holes grow much more rapidly than their host galaxies within the first billion years. However, there is a selection bias detailed in depth by Lauer et al. (2007) which suggests that the most luminous quasars will be biased to high black hole mass due to scatter in the correlation. In order to check whether this bias affects the conclusions of Wang et al. (2010) it is important to determine the black hole to galaxy mass relationship for the more common, lower luminosity quasars at $z \approx 6$ such as those identified in the Canada-France High-z Quasar Survey (CFHQS; Willott et al. 2010a).

An alternative approach to studying the co-evolution of galaxies and black holes is to determine the star formation rate of active galaxies over cosmic time (Carilli et al. 2001; Omont et al. 2003; Priddey et al. 2003; Wang et al. 2008, 2011a; Lutz et al. 2010; Serjeant et al. 2010; Bonfield et al. 2011; Omont et al. 2013). These studies suggest positive evolution in the star formation rate (SFR) at a fixed quasar luminosity from $z = 0$ to $z \approx 2$ and approximately constant or a mild decline at higher redshift. However, in these studies, most high-redshift quasars are undetected and conclusions have to be based on statistical detections of stacked sub-samples. ALMA now provides an opportunity to measure the SFR at least an order of magnitude fainter than previous observations and revolutionize our understanding of the co-evolution of black holes and their host galaxies.

In this paper we present an ALMA study of the interstellar medium of the host galaxies of two $z = 6.4$ CFHQS quasars. These quasars were selected for study based on their high redshift (they are two of the four highest redshift published quasars), faint absolute magnitude ($M_{1450} \geq -25$) and black hole masses of $\sim 10^8\,M_\odot$. Section 2 details the new observations. The results are presented in Section 3. Section 4 contains a discussion of the results. Cosmological parameters of $H_0 = 70$ km s^{-1} Mpc^{-1}, $\Omega_M = 0.27$ and $\Omega_\Lambda = 0.73$ (Komatsu et al. 2011) are assumed throughout.

2. OBSERVATIONS

CFHQS J021013-045620 (hereafter J0210-0456) and CFHQS J232908-030158 (hereafter J2329-0301) were observed with ALMA between June and August 2012 in *Early Science* project 2011.0.00243.S. The number of 12 m diameter antennae in use ranged from 17 to 24 with a typical longest baseline of 400 m. Observations of the science targets were interleaved with nearby phase calibrators, J0217+017 and J2323-032. Uranus was used as the amplitude calibrator and 3C446 as the bandpass calibrator. Total on-source integration times were 8000 s for J0210-0456 and 8500 s for J2329-0301.

The band 6 (1.3 mm) receivers were set up so that one of the four basebands (each of width 1.875 GHz) was centred on the expected location of the redshifted [C II] transition ($\nu_{\rm rest}$=1900.5369 GHz). The redshifts adopted were those of the low-ionization broad Mg II lines of the quasars measured by Willott et al. (2010b). Previous studies of high-redshift quasars have shown relatively small offsets (1σ dispersion 270 km s^{-1}) between Mg II and the systemic redshift (Richards et al. 2002). The remaining three spectral windows were placed nearby to sample the 1.2 mm continuum. Each baseband is sampled by 120 channels of width 15.625 MHz (equivalent to ≈ 18 km s^{-1}).

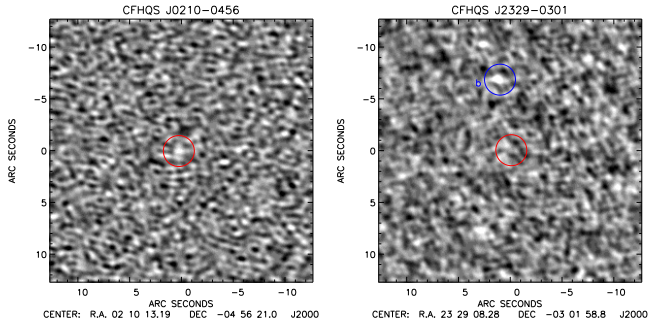

FIG. 1.— ALMA 1.2 mm continuum images generated from the three line-free basebands for each of the two quasar fields. The greyscale ranges from $-3\,\sigma$ (black) to $+3\,\sigma$ (white) where $\sigma = 35, 30\,\mu$Jy beam^{-1} for J0210-0456 (left) and J2329-0301 (right), respectively. Red circles show the expected source positions (circles do not indicate the positional uncertainty). There is a $3.4\,\sigma$ detection for J0210-0456 and no detection for J2329-0301. The strongest source in the field of J2329-0301 is marked with a blue circle and labelled 'b'. It is co-incident with a blue galaxy in the optical images of Willott et al. (2007).

Data processing was performed by staff at the North American ALMA Regional Center using the CASA software package[1]. The three line-free spectral windows were combined to generate 1.2 mm continuum images. Both the continuum maps and spectral line datacubes were spatially sampled with 0.″1 pixels. The synthesized beams are 0.″77 by 0.″52 for J0210-0456 and 0.″73 by 0.″63 for J2329-0301. The noise level reached in a 2 channel bin (31.25 MHz) is 0.22 mJy beam^{-1} for J0210-0456 and 0.23 mJy beam^{-1} for J2329-0301.

3. RESULTS

3.1. *Far-infrared luminosity*

The 1.2 mm continuum luminosity of $z = 6.4$ sources probes rest-frame 160 μm radiation, on the Rayleigh-Jeans tail side of the typical star-forming galaxy dust spectral energy distribution (SED; Lagache et al. 2005). This makes it an excellent proxy for the total far-infrared luminosity ($L_{\rm FIR}$; integrated luminosity over $42.5 - 122.5\,\mu$m) which is a reliable tracer of the star formation rate due to dust heated by young stars. In the most ultraviolet-luminous quasars (such as those at $z \sim 6$ in the SDSS), there is often a substantial contribution to $L_{\rm FIR}$ from dust heated by the AGN (Wang et al. 2008). The CFHQS quasars are an order of magnitude less UV-luminous than SDSS quasars and therefore should have a correspondingly lower contribution from AGN-heated dust, allowing continuum observations to probe lower star-formation rates.

The ALMA 1.2 mm continuum images generated from the three spectral windows that did not include the [C II] line were analyzed to determine their flux-densities. These images are shown in Figure 1 where the expected

[1] http://casa.nrao.edu

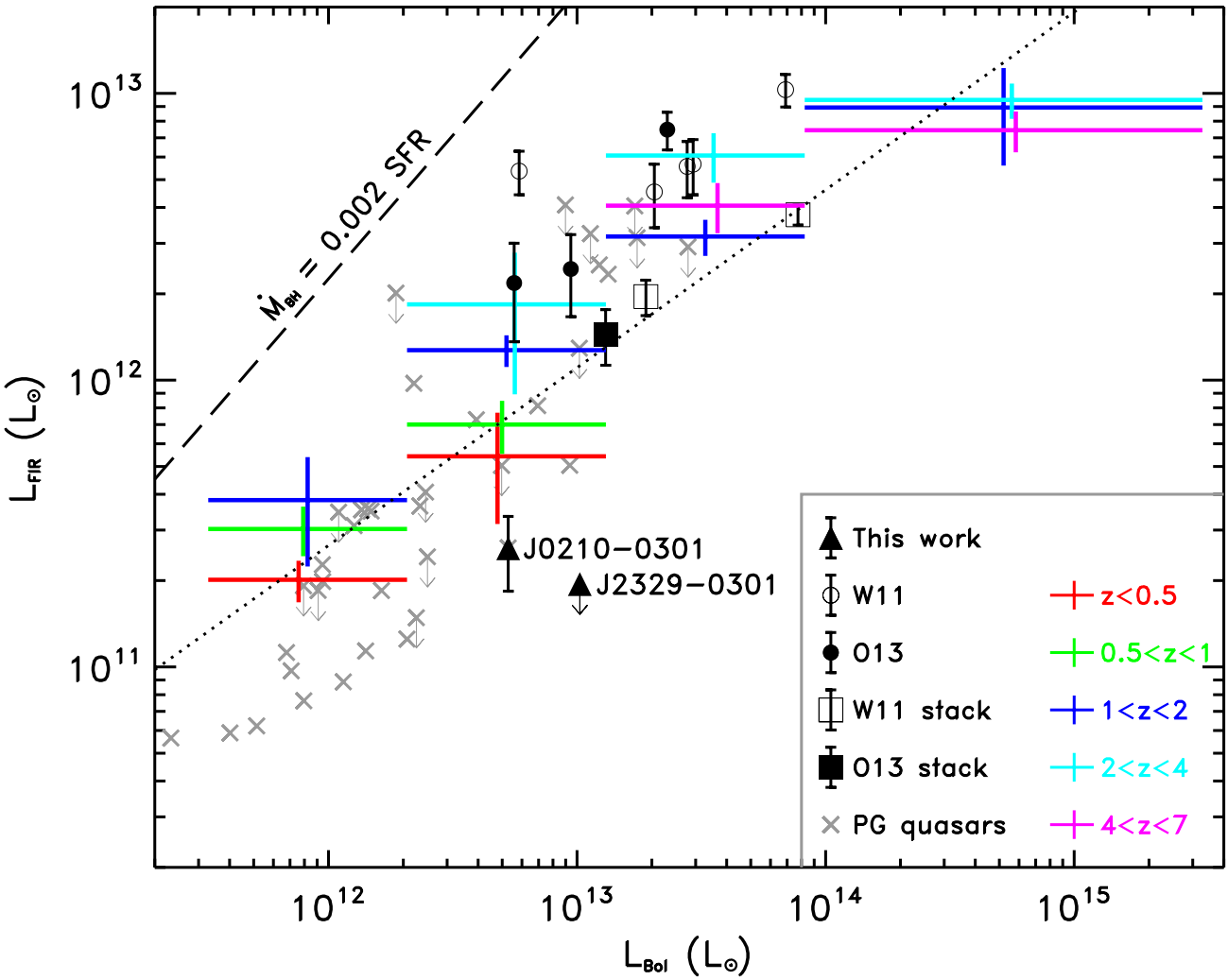

FIG. 2.— Far-infrared luminosity versus AGN bolometric luminosity for $z \approx 6$ quasars. The two CFHQS quasars observed with ALMA in this paper are shown with triangles. Previous detections from Wang et al. (2011a), mostly of SDSS quasars with a few quasars from other surveys, are shown as open circles. Previous detections of three CFHQS quasars are shown as filled circles (Omont et al. 2013). The squares show stacked averages from Wang et al. (2011a) and Omont et al. (2013). A complete sample of local PG quasars are shown with gray crosses (Hao et al. 2005). Colored lines show stacked averages in bins in redshift and $L_{\rm Bol}$ for quasars from the H-ATLAS survey and other far-IR/mm data (Serjeant et al. 2010). The dotted line is a fit to high-redshift ($2 < z < 7$) stack averages (Wang et al. 2011a). The dashed line converts $L_{\rm Bol}$ to black hole accretion rate and $L_{\rm FIR}$ to star formation rate such that these grow in parallel to match the local $M_{\rm BH}/M_{\rm stellar}$ relationship (Tundo et al. 2007).

locations of the quasars are identified by red circles. J0210-0456 is detected at 3.4σ with $f_{1.2\rm mm} = 120 \pm 35\,\mu$Jy. At this significance level it is not possible to determine whether the source is spatially resolved. J2329-0301 is undetected with no hint of positive flux at the quasar location. The most significant continuum source in the field (7″ north of the quasar, labeled 'b') is identified as a blue galaxy at much lower redshift in the optical imaging of Willott et al. (2007).

This continuum flux-density was converted to a far-infrared luminosity assuming a typical SED for high-redshift star-forming galaxies. To make meaningful comparison with previous results (in particular Wang et al. 2008; 2011a, Omont et al. 2013) we adopt a greybody spectrum with dust temperature, $T_{\rm d} = 47\,$K and emissivity index, $\beta = 1.6$. We note that our faint sources have much lower mm fluxes than the typical sources used to determine these parameters. If our sources instead have dust temperature closer to that of nearby luminous infrared galaxies (LIRGs, $10^{11} - 10^{12}\,{\rm L}_\odot, T_{\rm d} \approx 33\,$K, U et al. 2012) then the values of $L_{\rm FIR}$ would be 3× lower. For the remainder of this paper, uncertainties on $L_{\rm FIR}$ (and inferred SFR) only include the flux measurement uncertainties, not that of the dust temperature.

The far-IR luminosity of J0210-0456 is $(2.60 \pm 0.76) \times 10^{11}\,{\rm L}_\odot$. J2329-0301 is undetected with $L_{\rm FIR} < 1.9 \times 10^{11}\,{\rm L}_\odot$ (3σ limit). We note the incredible sensitivity of these early ALMA observations that reach the lower end of the LIRG classification in the early universe at $z = 6.4$.

We now consider the relationship between $L_{\rm FIR}$ and the quasar bolometric luminosity $L_{\rm Bol}$ for high-redshift quasars. $L_{\rm Bol}$ in this case is for the quasar component of the galaxy and assumes a typical bolometric correction from the rest-frame UV luminosity at 1450 Å of a factor of 4.4 (Richards et al. 2006). $L_{\rm Bol}$ does not include any excess FIR luminosity above that of the typical quasar. It is still a matter of debate as to how much of the typical quasar far-IR emission is due to dust heated by the AGN, compared to dust heated by a starburst (Haas et al. 2003;

Hao et al. 2005; Netzer et al. 2007; Lutz et al. 2010).

Because most high-redshift quasars have not been detected in mm continuum with the sensitivity level of previous studies, the relationship between $L_{\rm FIR}$ and $L_{\rm Bol}$ has been based on stacking of sub-samples with different bolometric luminosity ranges. Wang et al. (2011a) showed that the stacks based on several samples at $2 < z < 7$ could be fit by the relationship $L_{\rm FIR} \propto L_{\rm Bol}^{0.6}$. Omont et al. (2013) found that the stacked average from 1.2 mm MAMBO observations of CFHQS $z \approx 6$ quasars also lie on this relationship. The non-linear nature and significant scatter (for those detected so far) is interpreted in an evolutionary scenario where both star formation rate and black hole accretion are dependent upon dark matter halo mass, but with a lack of synchronization in the rates of these processes. The galaxies with the lowest $L_{\rm FIR}$ at a given $L_{\rm Bol}$ are expected to have a significant fraction of their $L_{\rm FIR}$ due to quasar-heated dust (Netzer et al. 2007).

Figure 2 shows previously published data for individually-detected $z \approx 6$ quasars and stacked averages from Wang et al. (2011a) and Omont et al (2013). The dotted line is the relationship between $L_{\rm FIR}$ and $L_{\rm Bol}$ found by Wang et al. (2011a) for stack averages of quasars at $2 < z < 7$. Note that both the stacked averages and relationship from Wang et al. 2011a have been renormalized according to the bolometric correction adopted here (see Omont et al. 2013 for more details). Gray crosses are a complete sample of low-redshift ($z < 0.5$) optically-selected Palomar-Green (PG) quasars (Hao et al. 2005). $L_{\rm FIR}$ for PG quasars has been estimated as $2\times$ the luminosity at 60 μm (Lawrence et al. 1989). Note that many of the highest luminosity (most distant) quasars in the PG sample are undetected at 60 μm and only have upper limits on $L_{\rm FIR}$. As noted by Wang et al. (2011a), the $z \approx 6$ stacked averages lie close to the correlation exhibited by low-redshift quasars, indicating no enhancement in SFR at high redshift for a given quasar luminosity.

Serjeant et al. (2010) used *Herschel* imaging of quasars in the H-ATLAS survey plus supplementary published IR and mm data to determine the average quasar far-infrared luminosity as a function of both redshift and quasar luminosity. Their data (for all bins containing 10 or more quasars) is shown in Figure 2 using an I band bolometric correction of 12.0 (Richards et al. 2006) and $L_{\rm FIR} = 1.75\times$ the luminosity at 100 μm. These data show a similar correlation of the two luminosities as found for the PG and $z \approx 6$ samples. However, Serjeant et al. do find a positive correlation between $L_{\rm FIR}$ and redshift up to $z \approx 3$ that does not continue up to the $z = 6$ data of Wang et al. (2011a) and Omont et al. (2013). A positive correlation between $L_{\rm FIR}$ and redshift up to $z \approx 2$ was also observed by Bonfield et al. (2011).

The values for the two CFHQS quasars with ALMA data are also plotted on Figure 2. The detection of J0210-0456 shows its $L_{\rm FIR}$ to be a factor of ≈ 3 lower than the stacked average relationship and below the stacked averages from H-ATLAS at all redshifts. The non-detection of J2329-0301 corresponds to $L_{\rm FIR}$ at least a factor of 10 lower than the stacked average from the full CFHQS sample (Omont et al. 2013) and substantially below the H-ATLAS averages.

The far-infrared luminosity can be used to derive the SFR assuming the relation in Kennicutt (1998) with a Salpeter (1955) initial mass function (IMF). For J0210-0456, SFR$= 48\,{\rm M}_\odot\,{\rm yr}^{-1}$ and for J2329-0301, SFR$< 40\,{\rm M}_\odot\,{\rm yr}^{-1}$ ($3\,\sigma$ limit). For both these objects, the assumption in deriving SFR is that there is no contribution to $L_{\rm FIR}$ from quasar-heated dust. These quasars lie close to the lower range of $L_{\rm FIR}$ where it has been suggested that the majority of the cool dust is heated by the quasar (Netzer et al. 2007). If this is the case then the SFR would be even lower. The very low SFR implied for the host galaxy of J2329-0301 is surprising given that it has a $2.5\times10^8\,{\rm M}_\odot$ black hole accreting at the Eddington rate (Willott et al. 2010b) and a very luminous, spatially-extended Lyα halo (Goto et al. 2009; Willott et al. 2011).

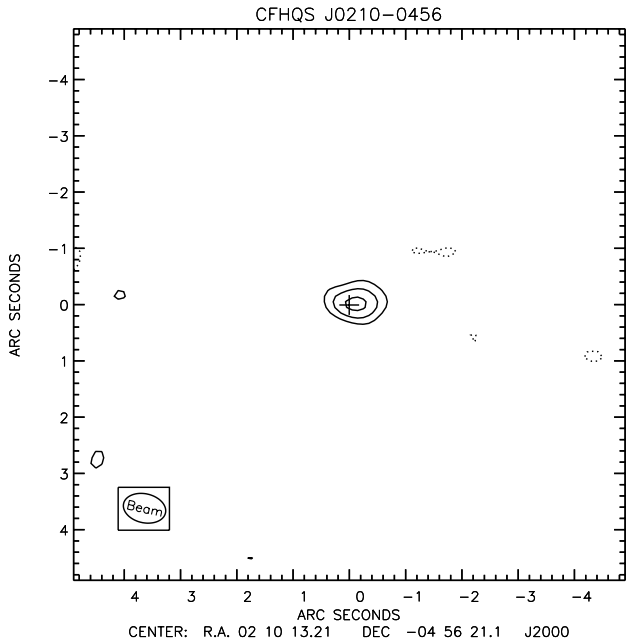

FIG. 3.— Continuum-subtracted [C II] line emission for CFHQS J0210-0456 integrated over 15 channels containing the [C II] line. Contours are at $[-3, 3, 5, 7]\times\sigma$ where $\sigma = 0.03\,{\rm Jy\,km\,s^{-1}\,beam^{-1}}$.

3.2. *[C II] luminosity*

The datacubes of the spectral windows containing the expected [C II] emission lines for the two quasars were inspected for line emission. A line was easily detected for J0210-0456, but not for J2329-0301. Figure 3 shows the image of [C II] emission for J0210-0456 integrated over the 15 channels (each of width 15.625 MHz) that show line emission. Continuum emission has been subtracted off using the continuum image of Figure 1. The source is elongated east-west, although note this is close to the major axis of the elongated beam. The spatial structure will be discussed further in the following section. No other [C II] emitters at the same redshift are seen in the field.

The spectrum of J0210-0456 is plotted in Figure 4. The [C II] line is offset from the broad ultraviolet Mg II emission line by $230\,{\rm km\,s^{-1}}$. Note that the rms observational uncertainty on the Mg II redshift is $160\,{\rm km\,s^{-1}}$, so the redshifts of [C II] and Mg II are consistent. We take the redshift of $z_{\rm [CII]} = 6.4323 \pm 0.0005$ to be the systemic redshift because it is measured to much higher accuracy

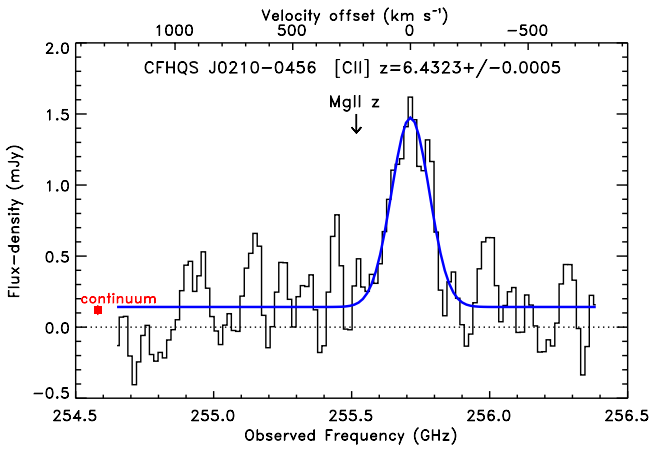

FIG. 4.— [C II] spectrum for CFHQS J0210-0456 overlaid with best fit Gaussian plus continuum model (blue). The red square with error bar is the continuum flux measured from the three line-free basebands. The arrow marked Mg II shows the redshift measured from the quasar broad line region.

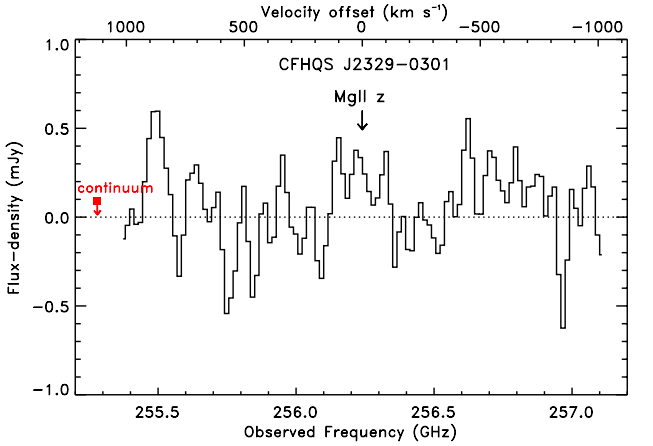

FIG. 5.— [C II] spectrum for CFHQS J2329-0301. There is no convincing detection of the line for this quasar. The red square with downward arrow is the limit on the continuum flux from the three line-free basebands.

than Mg II and is associated with star formation in the host galaxy rather than gas in the circum-quasar environment. A simple Gaussian plus constant fit was made to the observed spectrum. A Gaussian with FWHM $= 189 \pm 18\,\mathrm{km\,s^{-1}}$ provides a good fit to the line profile. The best-fit constant is positive showing a non-zero continuum level that is consistent with the continuum flux-density of $120\,\mu$Jy measured from the three line-free basebands in Section 3.1.

The improved systemic redshift for J0210-0456 allows an improvement in the determination of the size of the highly-ionized near-zone. The size of the region ionized by the quasar depends upon several factors including the neutral hydrogen fraction of the intergalactic medium when the quasar first turned on (Madau & Rees 2000; Cen & Haiman 2000) and therefore can be used to probe cosmic reionization. Willott et al. (2010b) used the Mg II redshift of this quasar to determine a near-zone size of 1.7 proper Mpc, which is lower than any other $z \approx 6$ quasar except for lineless or broad absorption line quasars (Fan et al. 2006; Carilli et al. 2010). Using the new redshift of $z_{[\mathrm{CII}]} = 6.4323$ gives a near-zone size of 1.4 proper Mpc, even lower than previously calculated. Correcting for the known luminosity-dependence of $R \propto L^{1/3}$ makes the size only slightly lower than the typical size for more luminous $z > 6.1$ quasars of 5 Mpc (Carilli et al. 2010).

The spectrum of J2329-0301 is plotted in Figure 5. It can be seen that there is not strong evidence for a measurable [C II] emission line. There is weak positive flux at the Mg II redshift that may correspond to real emission, but it is very uncertain so we assume here a non-detection.

The [C II] line flux of J0210-0456 was determined by integrating over the channels containing the line and subtracting off the continuum component. This line flux was then converted to a line luminosity at the measured redshift. For J2329-0301 a 3σ upper limit for the [C II] flux and luminosity was determined by assuming a spatially unresolved Gaussian with FWHM $= 300\,\mathrm{km\,s^{-1}}$. This line width is somewhat broader than that observed for J0210-0456 but narrower than CO line widths for SDSS $z \approx 6$ quasars (Wang et al. 2010). Measurements of emission line and continuum parameters derived from these data are quoted in Table 1.

TABLE 1
MILLIMETER DATA FOR CFHQS $z \approx 6.4$ QUASARS

	CFHQS J0210-0456	CFHQS J2329-0301
M_{BH}	$(8.0^{+5.5}_{-4.0}) \times 10^7 M_\odot$ [a]	$(2.5^{+0.4}_{-0.4}) \times 10^8 M_\odot$ [a]
z_{MgII}	6.438 ± 0.004 [a]	6.417 ± 0.002 [a]
$z_{[\mathrm{CII}]}$	6.4323 ± 0.0005	–
$\mathrm{FWHM}_{[\mathrm{CII}]}$	$189 \pm 18\,\mathrm{km\,s^{-1}}$	–
$I_{[\mathrm{CII}]}$	$0.269 \pm 0.037\,\mathrm{Jy\,km\,s^{-1}}$	$< 0.10\,\mathrm{Jy\,km\,s^{-1}}$ [b]
$L_{[\mathrm{CII}]}$	$(3.01 \pm 0.41) \times 10^8\,\mathrm{L_\odot}$	$< 1.1 \times 10^8\,\mathrm{L_\odot}$ [b]
$I_{\mathrm{CO}(2-1)}$	$< 0.014\,\mathrm{Jy\,km\,s^{-1}}$ [c]	–
$L_{\mathrm{CO}(2-1)}$	$< 1.6 \times 10^7\,\mathrm{L_\odot}$ [c]	–
$f_{1.2\mathrm{mm}}$	$120 \pm 35\,\mu$Jy	$< 90\,\mu$Jy [d]
L_{FIR}	$(2.60 \pm 0.76) \times 10^{11}\,\mathrm{L_\odot}$	$< 1.9 \times 10^{11}\,\mathrm{L_\odot}$ [d]
SFR	$48 \pm 14\,\mathrm{M_\odot\,yr^{-1}}$	$< 40\,\mathrm{M_\odot\,yr^{-1}}$ [d]
$L_{[\mathrm{CII}]}/L_{\mathrm{FIR}}$	$(1.15 \pm 0.32) \times 10^{-3}$	–
$L_{\mathrm{CO}(1-0)}/L_{\mathrm{FIR}}$	$< 8.5 \times 10^{-6}$	–

NOTES.—
[a] Derived from Mg II λ2799 observations (Willott et al. 2010b).
[b] 3σ upper limit assuming spatially unresolved and line width FWHM=300 km s^{-1}.
[c] 3σ upper limit from observations in Wang et al. (2011b) assuming spatially unresolved and FWZI=300 km s^{-1}.
[d] 3σ upper limit assuming spatially unresolved.

The [CII] line is primarily produced in photodissociation regions and is strongly dependent on the interstellar radiation field (Stacey et al. 1991). The ratio $L_{[\mathrm{CII}]}/L_{\mathrm{FIR}}$ has an inverse correlation on the radiation field strength and has been widely studied at lower redshift. It has been found that the ratio has an inverse correlation with L_{FIR} (Luhman et al. 2003). Graciá-Carpio et al. (2011) found this inverse correlation is even tighter if one normalises the far-IR luminosity by the molecular gas mass M_{H_2}. They attributed this to L_{FIR}/M_{H_2} being more closely related to the physical properties of the clouds such as density and temperature.

Figure 6 shows $L_{[\mathrm{CII}]}/L_{\mathrm{FIR}}$ against L_{FIR} for a compilation of low ($z < 0.4$) and high ($1 < z < 5$) redshift galaxies (Graciá-Carpio et al. 2011 and in prep.). The horizontal offset between the low and high redshift sources was attributed by Graciá-Carpio et al. (2011) to the higher molecular gas mass (for a given L_{FIR}) at high redshift (e.g. Tacconi et al. 2010). Also plotted on Fig-

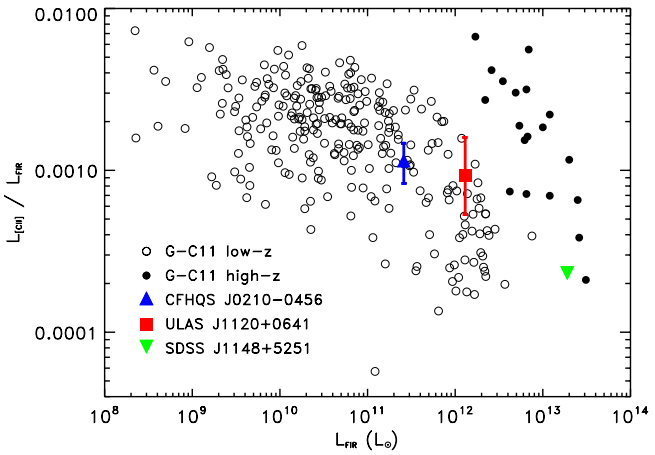

FIG. 6.— Ratio of [C II] to far-infrared luminosity versus far-infrared luminosity. Open circles show low-redshift ($z < 0.4$) and filled circles high-redshift ($1 < z < 5$) galaxies from the collection by Garciá-Carpio et al. (2011 and in prep.). Detections of quasars at $z > 6$ are shown individually: J0210-0456 (this paper), SDSS J1148+5251 (Maoilino et al. 2005) and ULAS J1120+0641 (Venemans et al. 2012). Note the outstanding high-redshift $L_{\rm FIR}$ sensitivity of ALMA in this *Early Science* observation with a modest integration time.

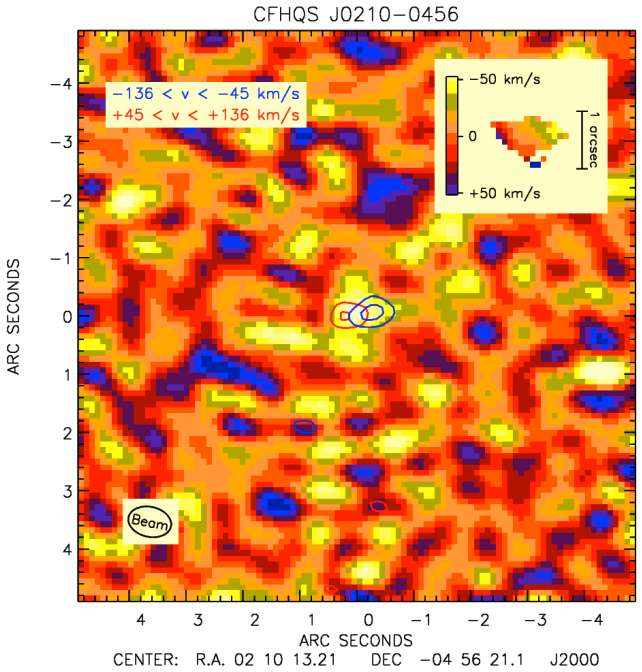

FIG. 7.— The background shows the continuum map of J0210-0456 and ranges from -3σ (purple) to $+3\sigma$ (yellow). The blue and red contours near the central dust continuum source show [C II] line emission maps for the blue ($-136 < v < -45\,{\rm km\,s^{-1}}$) and red ($+45 < v < +136\,{\rm km\,s^{-1}}$) wings, respectively. There is an offset of 0.″5 between these peaks, either side of the continuum centroid. The inset panel shows a [C II] peak velocity map for those pixels with sufficient flux to enable a Gaussian to be fitted. This map reveals a smooth velocity gradient across the source.

ure 6 are data for $z > 6$ quasars. SDSS J1148+5251 has a very high $L_{\rm FIR}$ and falls along the sequence of $2 < z < 5$ high-redshift galaxies (Maiolino et al. 2005). ULAS J1120+0641 (Venemans et al. 2012) and CFHQS J0210-0456 have more moderate $L_{\rm FIR}$ and fall within the region occupied by low-redshift galaxies. In the interpretation of the offset being due to higher molecular gas mass at high-redshift, this would suggest that not all high-redshift quasars exist in star-forming hosts with higher gas masses than at low redshift. The horizontal offset that is so striking in Figure 6 is at least partially due to a selection effect where previous facilities did not have the sensitivity to detect more moderate $L_{\rm FIR}$ at high redshifts and only ultraluminous continuum sources were followed up with [C II] observations. It is likely there is a large population of hitherto undetected high-redshift galaxies with properties like J0210-0456.

Wang et al. (2011b) reported Very Large Array observations aimed at detecting the CO $(2-1)$ emission from J0210-0456. The object was not detected and a line flux upper limit assuming a full-width zero-intensity of 800 ${\rm km\,s^{-1}}$ was reported. We have recalculated the line flux limit for the same width as the observed [C II] line (FWZI $= 300\,{\rm km\,s^{-1}}$). The 3σ upper limit on the line flux is then $< 0.014\,{\rm Jy\,km\,s^{-1}}$ giving a CO $(2-1)$ line luminosity limit of $L_{\rm CO(2-1)} < 1.6 \times 10^7\,{\rm L_\odot}$. To compare with other works that usually quote the ground-state CO transition we assume a luminosity ratio of CO $(2-1)$ / CO $(1-0) = 7.2$ (Stacey et al. 2010; Papadopoulos et al. 2012). Therefore the CO $(1-0)$ limit for J0210-0456 is $L_{\rm CO(1-0)} < 2.2 \times 10^6\,{\rm L_\odot}$ and the ratio $L_{\rm CO(1-0)}/L_{\rm FIR} < 8.5 \times 10^{-6}$. The limit on this ratio is an order of magnitude higher than the values for typical ultraluminous high-redshift galaxies and AGN (De Breuck et al. 2011) showing that much deeper observations are required to detect the molecular gas in galaxies such as these, highlighting how [C II] observations with ALMA are the best way to probe the obscured interstellar medium in typical high-redshift galaxies.

3.3. *[C II] dynamics and spatial extent*

Wang et al. (2010) showed that CO line widths of $z \approx 6$ SDSS quasars indicate ratios of black hole to galaxy mass typically a factor of 10 greater than in the local universe. This fits with the results presented in Section 3.1 where it was found that $z \approx 6$ quasar host galaxies are growing their black holes at a rate about $10\times$ faster than their stellar mass compared to the local ratio. In this work we have measured the [C II] line width for just one $z = 6.4$ quasar, so will only briefly discuss the ratio of black hole to dynamical mass at $z \approx 6$ and defer a fuller investigation until more $\sim 10^8\,{\rm M_\odot}$ black hole host galaxies have suitable mm interferometry data.

CFHQS J0210-0456 has a [C II] line FWHM of $189 \pm 18\,{\rm km\,s^{-1}}$, equivalent to $\sigma = 80 \pm 8\,{\rm km\,s^{-1}}$ for a Gaussian and ignoring any inclination correction. Based on the local relationship (Gultekin et al. 2009) a galaxy with $\sigma = 80\,{\rm km\,s^{-1}}$ would be expected to have $M_{\rm BH} \approx 3 \times 10^6\,{\rm M_\odot}$, a factor of 25 lower than the measured $M_{\rm BH} = 8 \times 10^7\,{\rm M_\odot}$. This difference is comparable to the factor of 10 found by Wang et al. for more luminous ($M_{\rm BH} \sim 10^9\,{\rm M_\odot}$) quasars. Even after taking account of possible inclination effects (Carilli & Wang 2006) this shows the black holes in $z \approx 6$ quasars to be considerably more massive than expected from the local relationship between black hole and galaxy mass.

To fully determine the gas kinematics requires spatially resolving the line emission. This should be possible with the full ALMA array that will offer spatial resolution reaching 20 milliarcseconds (mas), which is equivalent to 120 pc. Walter et al. (2009) found that the [C II] emission in SDSS J1148+5251 is concentrated within a radius of

only 750 pc of the nucleus. This is consistent with the small sizes of luminous $z \approx 6.5$ Lyman Break galaxies that have effective radii ≈ 800 pc (Ono et al. 2013).

The [C II] line image of J0210-0456 shown in Figure 3 shows elongation along an E-W direction, roughly aligned with the direction of the beam. The measured size of the source is 879 ± 55 mas $\times$ 642 ± 75 mas compared to a beam size of 770 mas $\times$ 520 mas. We used the CASA IMFIT task to fit a deconvolved model image to the data. This results in a deconvolved source of 521 ± 248 mas $\times$ 224 ± 297 mas oriented at a position angle of 128 degrees east of north. The intrinsic source size is not well constrained as it is only marginally resolved in this image comprised of all fifteen spectral channels of the [C II] line.

A different story emerges when one considers the blue and red sides of the [C II] line separately. Maps were made using only the red and blue wings (5 channels each) and excluding the centre of the line. Figure 7 shows the continuum dust emission as the background image. Superimposed on this are separate contours for the blue and red sides of the [C II] line. It can be seen that there is a spatial offset of $0\farcs5$ (3 kpc) between these peaks along a position angle similar to the 128 deg major axis of the marginally resolved full channel image. The inset panel of Figure 7 shows a velocity-centroid map of the [C II] line for pixels with sufficient flux to enable a Gaussian emission line to be fitted. There is a clear velocity gradient across the source along this same axis with magnitude ≈ 100 km s^{-1} across a size scale of $1\farcs0$ (6 kpc). Whether this is due to rotation of a galaxy wide disk or has a more complex origin in merging multiple components will require higher spatial resolution observations. This is similar to the [C II] velocity gradients over this scale observed by Wang et al. (2013) in some $z \sim 6$ SDSS quasars and quite different to the compact, intense, central starburst observed in SDSS J1148+5251 (Walter et al. 2009).

4. DISCUSSION

These observations with ALMA break new ground in their sensitivity to moderately star-forming galaxies at high-redshift. Even with this sensitivity, only one of the two $z \approx 6$ quasars was detected in line and continuum emission. The far-IR luminosity of J0210-0456 is $(2.60 \pm 0.76) \times 10^{11}$ L$_\odot$, whereas J2329-0301 remains undetected with $L_{\rm FIR} < 1.9 \times 10^{11}$ L$_\odot$, significantly below the typical far-IR luminosity for a quasar of this bolometric luminosity at any redshift. These low far-IR luminosities are surprising and place strong constraints on the star formation rates in the host galaxies of these Eddington-limited quasars.

In the simplest black hole/galaxy co-evolution scenario, cosmic stellar mass and black hole mass increase in lockstep, ending up at the ratio observed in the local universe of $M_{\rm BH}/M_{\rm stellar} = 0.002$ (Tundo et al. 2007). Detailed simulations show that in individual galaxies the phases of star formation and black hole accretion are not synchronized (Li et al. 2007) and this accounts for the significant scatter of points in Figure 2. It is trivial to calculate the relationship between star formation rate (linearly related to $L_{\rm FIR}$) and black hole accretion rate (linearly related to $L_{\rm Bol}$ and assuming an accretion efficiency of 10%) necessary to achieve $M_{\rm BH}/M_{\rm stellar} = 0.002$. This curve is plotted as the dashed line in the upper-left of Figure 2. All the optically-selected quasars observed at mm wavelengths are growing their black holes at a relatively faster pace than their stellar mass and this is not too surprising given that they were selected by their quasar emission. Galaxies should lie on both sides of the dashed line during their lifetimes in order to reach the local ratio at $z = 0$. At $z \approx 2$, mm-selected galaxies mostly lie to the upper left of the line showing that they are growing their stellar mass more rapidly than their black holes (Alexander et al. 2005). Lutz et al. (2010) also showed that low-luminosity AGN from deep X-ray surveys are found on the left side of such a line.

J2329-0301 is found to be growing its black hole at a rate of $> 100\times$ faster than its stellar mass in order to reach the local ratio. It has a black hole accretion rate of $\dot{M}_{\rm BH} \approx 7$ M$_\odot$ yr^{-1} and SFR < 40 M$_\odot$ yr^{-1} ($3\,\sigma$ limit, assuming $T_{\rm d} < 47$ K, no AGN-heated cool dust and Salpeter IMF). Khandai et al. (2012) report the results of hydrodynamic simulations of $z \sim 6$ quasar host galaxies. These show SFR that range from 100 to 1000 M$_\odot$ yr^{-1} as they evolve during the main black hole accretion phase. The simulations are designed to match the properties of the most luminous quasars from the SDSS. J2329-0301 has a black hole accretion rate $\sim 3\times$ lower than typical SDSS quasars and therefore scaling down the lowest simulated SFR by this amount would result in approximately the SFR limit observed for J2329-0301. This suggests that J2329-0301 is observed at a rare phase where it has very low SFR compared to its black hole accretion rate. In the Khandai et al. (2012) simulations, the SFR usually drops at the epoch of peak quasar accretion due to feedback heating the host galaxy gas. J2329-0301 appears to have very effectively shut off star formation. Although the far-IR data of high luminosity PG quasars has many non-detections and the H-ATLAS data are just stacked averages (Figure 2), it would appear that few low redshift quasars have such a low ratio of SFR to black hole accretion as J2329-0301. This quasar is known to be surrounded by a luminous Lyα halo at least 15 kpc across (Goto et al. 2009; Willott et al. 2011), which signifies a huge reservoir of diffuse gas likely photo-ionized by the quasar. When this gas cools and accretes on to the galaxy, a further bout of star formation is likely. Hayes et al. (2013) noted that the Lyα emission from galaxies with low dust content tends to be more extended than that in dusty galaxies, but do not provide a simple explanation for why this happens. J2329-0301 certainly fits this pattern with a low dust content as measured by thermal dust emission and a very extended Lyα halo.

The [C II] line detection in J0210-0456 is narrow (FWHM $= 189 \pm 18$ km s^{-1}) and shows only a small velocity gradient (≈ 100 km s^{-1}) across a scale of 6 kpc. The inclination angle of the [C II] emission is unconstrained, but the narrow line suggests the dynamical mass of the system is much lower than would be found in the local universe for a galaxy hosting a 10^8 M$_\odot$ black hole. This is in agreement with the results for more massive black holes at $z \approx 6$ (Wang et al. 2010) and fits with the discussion above that shows optically-selected $z \approx 6$ quasars have experienced enhanced black hole accretion relative to their stellar mass accumulation.

These early observations with ALMA are a prelude to increased resolution and sensitivity observations to come. A larger sample of $z \approx 6$ quasars with a wide range of

black hole masses is necessary to get a more complete picture of the relationship between black hole growth and star formation. Spatially resolved observations on scales of ~ 100 pc will reveal the dynamical state of the star forming gas and enable more accurate determination of dynamical masses.

Thanks to Javier Graciá-Carpio for providing unpublished far-IR data on the comparison sample of galaxies. Thanks to staff at the North America ALMA Regional Center for processing the ALMA data. Thanks to the anonymous referee for suggestions that improved the manuscript. This paper makes use of the following ALMA data: ADS/JAO.ALMA#2011.0.00243.S. ALMA is a partnership of ESO (representing its member states), NSF (USA) and NINS (Japan), together with NRC (Canada) and NSC and ASIAA (Taiwan), in cooperation with the Republic of Chile. The Joint ALMA Observatory is operated by ESO, AUI/NRAO and NAOJ. The National Radio Astronomy Observatory is a facility of the National Science Foundation operated under cooperative agreement by Associated Universities, Inc.

Facility: ALMA.

REFERENCES

Alexander, D. M., Smail, I., Bauer, F. E., et al. 2005, Nature, 434, 738
Blain, A. W., & Longair, M. S. 1993, MNRAS, 264, 509
Bonfield, D. G., Jarvis, M. J., Hardcastle, M. J., et al. 2011, MNRAS, 416, 13
Bouwens, R. J., Illingworth, G. D., Blakeslee, J. P., & Franx, M. 2006, ApJ, 653, 53
Carilli, C. L., Bertoldi, F., Rupen, M. P., et al. 2001, ApJ, 555, 625
Carilli, C. L., & Wang, R. 2006, AJ, 131, 2763
Carilli, C. L., Wang, R., Fan, X., et al. 2010, ApJ, 714, 834
Carilli, C. L., Riechers, D., Walter, F., Maiolino, R., Wagg, J., Lentati, L., McMahon, R., & Wolfe, A. 2013, ApJ, 763, 120
Carilli, C. L., & Walter, F. 2013, ARA&A, in press, arXiv:1301.0371
Cattaneo, A., Faber, S. M., Binney, J., et al. 2009, Nature, 460, 213
Cen, R., & Haiman, Z. 2000, ApJ, 542, L75
De Breuck, C., Maiolino, R., Caselli, P., Coppin, K., Hailey-Dunsheath, S., & Nagao, T. 2011, A&A, 530, L8
Fan, X., Strauss, M. A., Becker, R. H., et al. 2006, AJ, 132, 117
Ferrarese, L., & Merritt D. 2000, ApJ, 539, L9
Goto, T., Utsumi, Y., Furusawa, H., Miyazaki, S., & Komiyama, Y. 2009, MNRAS, 400, 843 (G09)
Graciá-Carpio, J., Sturm, E., Hailey-Dunsheath, S., et al., 2011, ApJ, 728L, 7
Gultekin, K., Richstone, D. O., Gebhardt, K., et al. 2009, ApJ, 698, 198
Haas, M., Klaas, U., Muller, S. A. H., et al. 2003, A&A, 402, 87
Hao, C. N., Xia, X. Y., Mao, S., Wu, H., & Deng, Z. G. 2005, ApJ,625, 78
Hayes, M., Ostlin, G., Schaerer, D., et al. 2013, ApJ, 765L, 27
Kennicutt, R. C., Jr. 1998, ARA&A, 36, 189
Khandai, N., Feng, Y., DeGraf, C., Di Matteo, T., & Croft, R. A. C. 2012, MNRAS, 423, 2397
Komatsu, E., Smith, K. M., Dunkley, J., et al. 2011, ApJS, 192, 18
Lagache, G., Puget, J., & Dole, H. 2005, ARA&A, 43, 727
Lawrence, A., Rowan-Robinson, M., Leech, K., Jones, D. H. P., & Wall, J. V. 1989, MNRAS, 240, 329
Lauer, T. R., Tremaine, S., Richstone, D., & Faber, S. M. 2007, ApJ, 670, 249
Li, Y., Hernquist, L., Robertson, B., et al. 2007, ApJ, 665, 187
Luhman, M. L., Satyapal, S., Fischer, J., et al. 2003, ApJ, 594, 758
Lutz, D., Mainieri, V., Rafferty, D., et al. 2010, ApJ, 712, 1287
Madau, P., & Rees, M. J. 2000, ApJ, 542L, 69
Magorrian, J., Tremaine, S., Richstone, D., et al. 1998, AJ, 115, 2285
Maiolino, R., Cox, P., Caselli, P., et al. 2005, A&A, 440, L51
Mechtley, M., Windhorst, R. A., Ryan, R. E., et al. 2012, ApJ, 756L, 38
Netzer, H., Lutz, D., Schweitzer, M., et al. 2007, ApJ, 666, 806
Omont, A., Beelen, A., Bertoldi, F., Cox, P., Priddey, R. S., McMahon, R. G., & Isaak, K. G. 2003, A&A, 398, 857
Omont, A., Willott, C. J., Beelen, A., Bergeron, J., Orellana, G., & Delorme, P. 2013, A&A, 552A, 43
Ono, Y., Ouchi, M., Curtis-Lake, E., et al. 2013, ApJ, submitted, arXiv:1212.3869
Papadopoulos, P. P., van der Werf, P., Xilouris, E. M., et al. 2012, MNRAS, 426, 2601
Priddey, R. S., Isaak, K. G., McMahon, R. G., & Omont, A. 2003, MNRAS, 339, 1183
Reddy, N. A., & Steidel, C. C. 2009, ApJ, 692, 778
Richards, G. T., Vanden Berk, D. E., Reichard, T. A., Hall, P. B., Schneider, D. P., SubbaRao, M., Thakar, A. R., & York, D. G. 2002, AJ, 124, 1
Richards, G. T., Lacy, M., Storrie-Lombardi, L. J., et al. 2006, ApJS, 166, 470
Salpeter, E. E. 1955, ApJ, 121, 161
Serjeant, S., Bertoldi, F., Blain, A. W., et al. 2010, A&A, 518, L7
Stacey, G. J., Geis, N., Genzel, R., et al. 1991. ApJ, 373, 423
Stacey, G. J., Hailey-Dunsheath, S., Ferkinhoff, C., et al. 2010. ApJ, 724, 957
Tacconi, L. J., Genzel, R., Neri, R., et al. 2010, Nature, 463, 781
Tanvir, N. R., Levan, A. J., Fruchter, A. S., et al. 2012, ApJ, 754, 46
Tundo, E., Bernardi, M., Hyde, J. B., Sheth, R. K., & Pizzella, A. 2007, ApJ, 663, 53
U, V., Sanders, D. B., Mazzarella, J. M., et al. 2012, ApJS, 203, 9
Venemans, B. P., McMahon, R., Walter, F., et al. 2012. ApJ, 751, L25
Wagg, J., Wiklind, T., Carilli, C.L., et al. 2012, ApJ, 752, L30
Walter, F., Carilli, C. L., Bertoldi, F. et al. 2004, ApJ, 615, L17
Walter, F., & Carilli, C. L. 2008, Ap&SS, 313, 313
Walter, F., Riechers, D., Cox, P., et al. 2009, Nature, 457, 699
Wandel, A. 1999, ApJ, 519, L39
Wang, R., Wagg, J., Carilli, C. L., et al. 2008, AJ, 135, 1201
Wang, R., Carilli, C. L., Neri, R., et al. 2010, ApJ, 714, 699
Wang, R., Wagg, J., Carilli, C. L., et al. 2011a, AJ, 142, 101
Wang, R., Wagg, J., Carilli, C. L., et al. 2011b, ApJ, 739, L34
Wang, R., Wagg, J., Carilli, C. L., et al. 2013, arXiv:1210.0242, IAU Symposium No. 292, "Molecular Gas, Dust, and Star Formation in Galaxies".
Willott, C. J., Delorme, P., Omont, A., et al. 2007, AJ, 134, 2435
Willott, C. J., Delorme, P., Reylé, C., et al. 2010a, AJ, 139, 906
Willott, C. J., Albert, L., Arzoumanian, D., et al. 2010b, AJ, 140, 546
Willott, C. J., Chet, S., Bergeron, J., & Hutchings, J. B. 2011, AJ, 142, 186